# Accepted Manuscript


The H-bond network surrounding the pyranopterins modulates redox cooperativity in the molybdenum-*bis*PGD cofactor in arsenite oxidase

Simon Duval, Joanne M. Santini, David Lemaire, Florence Chaspoul, Michael J. Russell, Stephane Grimaldi, Wolfgang Nitschke, Barbara Schoepp-Cothenet

PII: S0005-2728(16)30523-0
DOI: doi: 10.1016/j.bbabio.2016.05.003
Reference: BBABIO 47688

To appear in: *BBA - Bioenergetics*

Received date: 9 October 2015
Revised date: 12 May 2016
Accepted date: 16 May 2016

Please cite this article as: Simon Duval, Joanne M. Santini, David Lemaire, Florence Chaspoul, Michael J. Russell, Stephane Grimaldi, Wolfgang Nitschke, Barbara Schoepp-Cothenet, The H-bond network surrounding the pyranopterins modulates redox cooperativity in the molybdenum-*bis*PGD cofactor in arsenite oxidase, *BBA - Bioenergetics* (2016), doi: 10.1016/j.bbabio.2016.05.003

# The H-bond network surrounding the pyranopterins modulates redox cooperativity in the molybdenum-*bis*PGD cofactor in arsenite oxidase

Simon Duval[a], Joanne M. Santini[b], David Lemaire[c], Florence Chaspoul[d], Michael J. Russell[e], Stephane Grimaldi[a], Wolfgang Nitschke[a], and Barbara Schoepp-Cothenet[a,1]

[a]CNRS, Aix-Marseille Univ, BIP UMR 7281, IMM FR 3479, 31 chemin J. Aiguier, 13402 Marseille Cedex 20, France

[b]Institute of Structural and Molecular Biology, University College London, WC 1E 6BT, UK

[c]Institut de Biologie Environnementale et Biotechnologie, CEA de Cadarache, 13108 Saint Paul Lez Durance Cedex, France

[d]IMBE Aix Marseille Université, IRD CNRS UAPV , Faculté de Pharmacie, 13005 Marseille, France

[e]Jet Propulsion Laboratory, California Institute of Technology, 4800 Oak Grove Drive, Pasadena, CA91109-8099, USA

[1]Contact Informations: Barbara Schoepp-Cothenet ; CNRS, Aix-Marseille Univ, BIP UMR 7281, IMM FR 3479, 31 chemin J. Aiguier, 13402 Marseille Cedex 20, France ; Tel : +33491164672 ; schoepp@imm.cnrs.fr.

**Abreviations** :

Aio: arsenite oxidase; AMPSO: 3-([1,1-Dimethyl-2-hydroxyethyl]amino)-2-hydroxypropanesulfonic acid; EPR: Electron Paramagnetic Resonance; HEPES: 4-(2-hydroxyethyl)-1-piperazineethanesulfonic acid ; $K_s$: stability constant; MES: 2-(*N*-morpholino)ethanesulfonic acid ; Mo: Molybdenum; MOPS: 3-(*N*-morpholino)propanesulfonic acid; PGD: Pyranopterin Guanosine Dinucleotide.

**Abstract**

While the molybdenum cofactor in the majority of *bis*PGD enzymes goes through two consecutive 1-electron redox transitions, previous protein-film voltammetric results indicated the possibility of cooperative (n=2) redox behavior in the bioenergetic enzyme arsenite oxidase (Aio). Combining equilibrium redox titrations, optical and EPR spectroscopies on concentrated samples obtained *via* heterologous expression, we unambiguously confirm this claim and quantify Aio's redox cooperativity. The stability constant, $K_s$, of the $Mo^V$ semi-reduced intermediate is found to be lower than $10^{-3}$. Site-directed mutagenesis of residues in the vicinity of the Mo-cofactor demonstrates that the degree of redox cooperativity is sensitive to H-bonding interactions between the pyranopterin moieties and amino acid residues. Remarkably, in particular replacing the Gln-726 residue by Gly results in stabilization of (low-temperature) EPR-observable $Mo^V$ with $K_S = 4$. As evidenced by comparison of room temperature optical and low temperature EPR titrations, the degree of stabilization is temperature-dependent. This highlights the importance of room-temperature redox characterizations for correctly interpreting catalytic properties in this group of enzymes.

Geochemical and phylogenetic data strongly indicate that molybdenum played an essential biocatalytic roles in early life. Molybdenum's redox versatility and in particular the ability to show cooperative (n=2) redox behavior provide a rationale for its paramount catalytic importance throughout the evolutionary history of life. Implications of the H-bonding network modulating Molybdenum's redox properties on details of a putative inorganic metabolism at life's origin are discussed.

**Keywords**: Arsenite oxidase; Molybdenum enzyme; optical spectroscopy; EPR spectroscopy; redox titrations;

## 1. Introduction

In prokaryotes, the enzyme arsenite oxidase (Aio), a member of the vast superfamily of the so-called Molybdenum-*bis*Pyranopterin Guanosine Dinucleotide (Mo-*bis*PGD) enzymes (previously denoted as the DMSO-reductase or CISM-superfamily [1, 2]), injects reducing equivalents derived from the oxidation of arsenite into a variety of chemiosmotic electron transfer chains [3]. In addition to the catalytic Mo-*bis*PGD cofactor, the enzyme features a cubane-type iron sulfur center harbored by the large catalytic subunit and a Rieske-type [2Fe-2S] cluster ligated within the smaller subunit of the heterodimeric enzyme [4, 5]. The cubane-type cluster in Aio is a [3Fe-4S] cluster whereas this cofactor mostly corresponds to a [4Fe-4S] center in other members of the superfamily. The small subunit with its Rieske-type center is specific to Aio and not found in other families of Mo-*bis*PGD enzymes. While the catalytic molybdenum centers present in the majority of Mo-*bis*PGD enzymes commonly shuttle through two distinct redox transitions ($Mo^{VI}/Mo^{V}$ and $Mo^{V}/Mo^{IV}$) featuring a paramagnetic $Mo^{V}$ state observable by Electron Paramagnetic Resonance (EPR)[6-11], no such $Mo^{V}$ EPR signals were observed in Aio. The report of n=2 behavior in Aio from *Alcaligenes* (*A.*) *faecalis* as observed by protein film voltammetry (PFV) [12] eventually proposed a rationale for the seemingly missing $Mo^{V}$ EPR signal. Parts of the results from the initial PFV study were subsequently challenged in an independent study applying the same method to an Aio from a different organism, *Rhizobium* (*R.*) sp. Str. NT-26 [13].

In this work, we address the question of the Mo-cofactor's redox behavior in Aio by redox titrations monitoring (a) the $Mo^{VI}$ state by optical spectroscopy and (b) the (1-electron reduced) $Mo^{V}$ state by EPR. No EPR redox titrations on Aio have been published so far and no optical titrations have yet been performed on any member of the superfamily. Our results

confirm the results obtained by Hoke *et al.* [12] and definitively show that the Mo-*bis*PGD center in Aio undergoes a positively cooperative (n=2) 2-electron transition with two protons strongly coupled to the redox event. In contrast to PFV, our experimental approach furthermore allowed for the determination of an upper limit for the stability constant ($K_S$) of the semi-reduced $Mo^V$ state. Expressing the redox properties of Aio and of other Mo-*bis*PGD enzymes in terms of $K_S$ of the $Mo^V$ state permits a quantitative comparison of the Mo-*bis*PGD cofactors to quinone-based systems in a common formalistic framework.

The existence of both positive (in Aio) and negative redox cooperativity (in several other Mo-*bis*PGD enzymes) in the Mo-pterin cofactors' redox titrations raises the question of the parameters steering the center into one or the other redox regime. To assess these parameters, we have produced and characterized site-directed variants of Aio targeting both the immediate ligand-sphere of the metal and the environment of the coordinating pterin. Only a mutation affecting the pterins was found to substantially stabilize an EPR-detectable $Mo^V$ state and thus to shift Aio's redox behavior from strongly positive towards more negative cooperativity.

## 2. Experimental Procedures

### *2.1. Bacterial strains, plasmid and growth conditions*

The *aioBA* genes of Aio were cloned without the *aioB* Tat leader sequence into pPROEX-HTb (Invitrogen) and expressed in *Escherichia* (*E.*) *coli* DH5α growing aerobically as already described [5].

### *2.2. Site-directed mutagenesis*

The primers used to create point mutations in the *aioA* gene are shown in Table S1. Variants were made using the Agilent Quick Change II XL site-directed mutagenesis kit according to manufacturer's instructions as has been done previously [5]. Mutations were confirmed by sequencing both strands.

*2.3. Proteins purification*

The WT and variant Aio proteins from *R.* sp. NT-26 and WT Aio from *A. faecalis* were heterologously expressed in *E. coli* and purified according to a protocol adapted from [5]. The 50 mM MES, 150 mM NaCl (pH5.5) equilibration buffer of the Superdex 200 10/300 gel filtration column (GE Healthcare) was replaced by a 30 mM MES/30 mM Tricine/30 mM HEPES/30 mM AMPSO/300 mM NaCl, pH 6-9 mix buffer. The presence of 300 mM NaCl has been found to improve protein stability. The *E. coli* NarGH was expressed using the plasmid pNarGHHis$_6$J, purified in one step by affinity chromatography as described previously [14] and finally recovered in 50 mM MOPS pH7.6 buffer at 90 μM.

*2.4. Enzyme Assay*

Arsenite oxidase enzyme assays were done as described previously [5], using the artificial electron acceptor, 2,6-dichlorophenolindophenol (DCPIP) 200 μM combined with phenazine methosulfate (PMS) in 50 mM MES (pH 6) or using horse cytochrome *c* in 50 mM Tricine (pH 8).

*2.5. Optical titrations*

Optical equilibrium redox titrations were performed on purified enzyme obtained from a 2 liter-culture and diluted in the mix buffer with pH-values adjusted to 6-9. Enzyme concentrations were approximately 40 μM. Each reductive/oxidative titration was performed twice with two separate preparations at each pH value. The titrations were performed at 13°C [15] using a Cary 5E UV/Vis spectrophotometer, under Argon atmosphere in the presence of the following redox mediators at 10 μM: Ferrocene, 1,4 *p*-benzoquinone, 2,5-dimethyl-*p*-benzoquinone, 2-hydroxy 1,2-naphthoquinone, 1,4-naphthoquinone. Titrations were carried out using sodium ascorbate for reduction, and potassium ferricyanide for oxidation. Samples were allowed to equilibrate for several minutes. The redox midpoint potential values of the Mo cofactor were determined by evaluating the change in absorbance at 695 nm after normalizing the spectra to zero at 800 nm to correct for baseline changes between individual spectra. Due to the comparatively low extinction coefficients (ε) of the $Mo^{V}$ and the $Mo^{IV}$ states, this normalization procedure only affects the $\varepsilon_{695}$ of the $Mo^{VI}$ state while leaving the Beer-Lambert dependency on $Mo^{VI}$ concentration unaltered. The data were fitted to a Nernstian sigmoid with n = 2 or n = 1 transitions.

*2.6. Electron Paramagnetic Resonance*

EPR spectroscopy was performed on purified enzymes in the mix buffer (pH 6 or 7) with approximately 40 μM enzyme. During the equilibrium redox titration, the redox potential was poised at 10°C as described in Duval [16], in the presence of the following redox mediators at 100 μM: 1,4 *p*-benzoquinone, 2,5-dimethyl-*p*-benzoquinone, 2-hydroxy 1,2-naphthoquinone, 1,4-naphthoquinone. Titrations were carried out using ascorbate for reduction, and ferricyanide for oxidation. Samples were allowed to equilibrate for several minutes. EPR spectra were recorded on a Bruker ElexSys X-band spectrometer fitted with an Oxford

Instruments liquid-Helium cryostat and temperature control system. The EPR spectra of Aio (WT: 32 scans; Q726G variant: 396 scans) were measured at differing temperatures (12 K to 50 K), microwave powers (0.51 µW to 1 mW), and modulation amplitudes (0.4 mT to 1.0 mT) to optimize signal amplitudes of the assayed cofactors. The EPR spectrum (1 scan) of NarGH was recorded at 1 mW, 0.4 mT modulation amplitude and at 50K.

*2.7. ESI/MS Analysis*

All mutations were confirmed by mass spectrometry performed on purified enzymes. Analyses were performed on a MicroTOF-Q (Bruker) with an electrospray ionization source. Samples were desalted and concentrated in 20mM ammonium acetate buffer prior to analyses with Centricon Amicon with a cut off of 30kDa. Samples were diluted with $CH_3CN/H_2O$ (1/1-v/v), 0.2% formic acid and were continuously infused at a flow rate of 3 µL/min. Mass spectra were recorded in the 50-7000 mass-to-charge (*m/z*) range. MS experiments were carried out with a capillary voltage set at 4.5 kV and an end-plate offset voltage at 500 V. The gas nebulizer ($N_2$) pressure was set at 0.4 bar and the dry gas flow ($N_2$) at 4 L/min at a temperature of 190 °C. Data were acquired in the positive mode and calibration was performed using a calibrating solution of ESI Tune Mix in $CH_3CN/H_2O$ (95/5-v/v). The system was controlled with the software package MicrOTOF Control 2.2 and data were processed with DataAnalysis 3.4.

*2.8. ICP/MS Analysis*

Molybdenum concentrations were determined in all purified enzymes by ICP/MS. Prior to the analysis, samples were mineralized in a mixture containing 2/3 of nitric acid (65 % Purissime)

and 1/3 of hydrochloric acid (37%, Trace Select). Samples were diluted five-fold before ICP/MS analysis. The ICP-MS instrument was an ICAP Q (ThermoElectron), equipped with a collision cell. The calibration curve was obtained by dilution of a certified multi-element solution. Molybdenum concentrations were determined using Plasmalab software, at a mass of interest m/z=95.

## 3. Results

Two X-ray crystal structures of Aio from two members of the Proteobacteria *A. faecalis* and *R.* sp. str. NT-26 [4, 5], have been determined. Strong conservation of structure between both enzymes in particular in the vicinity of the Mo-center was observed [5]. However, when studied with respect to their electrochemical properties, these two enzymes were reported to differ substantially [12, 13]. In the *A. faecalis* Aio, the Mo-*bis*PGD center was found to display a strongly positive cooperative 2-electron redox transition with a midpoint potential slightly below +300 mV at pH 6 and a pH-dependence thereof indicating the strong coupling of two protons to the redox event [12] (represented by the dashed red line in Fig. 1). In contrast, the enzyme from *R.* sp. NT-26 was reported to feature a higher (by almost 100 mV) redox potential and a pH-dependence corresponding to only one proton per two electrons [13] (Fig. 1, dashed blue line). Our first goal therefore was to clarify these divergences.

### *3.1. Re-examination of divergent electrochemical data on the Mo-bisPGD cofactor in the Aio from A. faecalis and R. sp. NT-26*

Rather than by the voltammetric method, redox changes of Mo centers traditionally are followed *via* the EPR signal of the 1-electron-reduced, paramagnetic $Mo^V$ state. However, no $Mo^V$ EPR signal has so far been detected in Aio [17], a fact which would find a straightforward rationalization in the cooperative 2-electron redox behavior proposed by Hoke *et al*. [12] implying a highly destabilized semi-reduced intermediate state. We therefore resorted to optical spectroscopy. The UV/Vis absorption spectra of the molybdenum cofactor in these Mo-*bis*PGD enzymes, however, are broad and feature low extinction coefficients. Optical redox titrations therefore require high sample concentrations and consequently are rarely performed. To the best of our knowledge, the DMSO reductase Dor from *Rhodobacter sphaeroides* was, prior to this work, the only Mo-*bis*PGD enzyme intensively studied by optical spectroscopy with the aim to establish the redox properties of the Mo-center [18]. However, even in Dor, optical spectroscopy was not used to directly monitor equilibrium redox titrations of the Mo center.

Fig. 2A shows oxidized-minus-reduced difference spectra measured on the *R.* sp. NT-26 enzyme in a range of ambient potentials. These spectra closely resemble that of the native enzyme from *A. faecalis* [17] (for the full wavelength range spectrum, see Fig. S1A). The Mo-center strongly contributes to the spectrum in the 600 to 800 nm range (as already shown for DMSO reductase [18]), with a broad peak at 695 nm (Fig. 2A) on which we evaluated the Mo cofactor's $E_m$ values. In this spectral region, the absorbance of the two iron-sulfur centers is negligible. The recorded data closely correspond to an n=2 Nernst curve (Fig. 2B, blue trace) but cannot be explained by a single-electron n=1 transition (red curve) and an $E_{m,pH6}$ value of +240 ±10 mV was obtained. All titration waves in the pH range from 6 to 9 correspond to such 2-electron transitions (Fig. S1B), although the data obtained at pH 9 admittedly show a higher scatter than at other pH values due to progressive degradation of the sample. In this pH range, the difference spectra of the wild-type (WT) enzyme show no obvious contributions

from a $Mo^V$ state characterized by a prominent feature at 500/550 nm in the enzyme Dor [18]. No significant amount of $Mo^V$ can be detected by EPR throughout the addressed pH range (see below and Figure 3). The pH dependence of the observed n=2 transitions (see also Table 1) has a uniform slope of -50 ±10 mV/pH unit over the assayed pH range (Fig. 1 our data points are indicated by blue squares and the deduced regression curve is shown as a continuous blue line), in line with the theoretical value of -56 mV per pH unit expected at 13 °C for a strongly proton-coupled electron transfer and an $H^+/e^-$ ratio of 1.

As shown in Fig. 1, the $E_m$-values and pH dependences thereof in Aio from *R.* sp. NT-26 (continuous blue line and blue squares, respectively) closely match the results obtained on the native enzyme from *A. faecalis* (dashed red line, [12]) whereas they differ substantially from those reported for the native enzyme from *R.* sp. NT-26 [13] (dashed blue line). Since we used the recombinant *R.* sp. NT-26 enzyme, it was necessary to assess whether the observed differences were a result of the heterologous expression system. We consequently performed the characterization of the expressed *A. faecalis* enzyme in our high-yield system. The values obtained from the redox titrations (Fig. S1C) are shown in Fig. 1 (orange triangles) and correspond well to the data by Hoke *et al.* [12] measured on the native enzyme (dashed red line). The Mo centers in the WT Aios from *A. faecalis* and *R.* sp. NT-26 therefore behave similarly both with respect to redox potential and to pH dependence thereof. The divergent results reported in [13] (as illustrated by the dashed blue line in Fig. 1 lying substantially above all other data and featuring a different slope) could not be reproduced in our experiments. Overall it can be concluded that both systems undergo strongly proton-coupled n=2 redox transitions.

*3.2. A quantitative measure of redox cooperativity in 2-electron transitions*

We therefore conclude that the 2-electron redox transition in Aio features strongly positive cooperativity, *i.e.* the first reduction step renders the second one very oxidizing resulting in a simultaneous uptake of two electrons and *vice versa* for the oxidizing direction. Intuitively, one might expect that, by virtue of electrostatic repulsion, the negative charge of the first electron must push the second reduction step towards lower redox potentials. This is indeed what is observed in many cases and what is referred to as "negative redox cooperativity". Negative redox cooperativity characterizes the behavior of many multi-center redox proteins (e.g. see [19]) corresponding to electrostatic effects of the first redox event on the second one. Rare cases of positive cooperativity have also been reported and have been rationalized by redox-induced conformational changes [20]. The emblematic examples for positive redox cooperativity, however, are the 2-electron transitions of quinones in aqueous solutions. A quantitative description of redox cooperativity in general was developed by Michaelis [21]. A more general presentation of the mathematical description together with numerous examples from organic chemistry was provided by Clark [22]. An introduction to the conceptual framework of cooperative 2-electron redox chemistry is presented in the Supplemental Material. This formalism emphasizes that the regimes of positive and negative cooperativity actually form a continuum with a smooth transition between the two extremes. In the region of negative cooperativity the transition from the fully oxidized to the 1-electron reduced form ($E_1$) occurs at substantially more positive potentials than that of the subsequent transition to the fully reduced state ($E_2$) ([21, 22]). The individual 1-electron transitions can therefore be directly observed and their $E_1$ and $E_2$ values determined (see Fig. S2A). By contrast, in a redox reaction with strong positive cooperativity $E_1$ is much lower than $E_2$ , resulting in the simultaneous uptake/loss of two electrons, and the titration wave will within experimental accuracy resemble a single n=2 Nernst curve (Fig. S2D). The latter case is precisely what we observe in the titration curve of the fully oxidized $Mo^{VI}$ state in Aio (Fig.

2B). Fig. S2, however, also illustrates that for $\Delta E = E_1-E_2$ in the vicinity of 0 (Figs. S2B and S2C), the theoretical titration curves of the fully oxidized state deviate from both the n=1 and the n=2 dependences in principle allowing experimental access to ΔE. The scatter of our experimental data points (Fig. 2B), however, renders this kind of approach insufficient for ΔE value determinations prompting us to use EPR monitoring of the paramagnetic $Mo^V$ state to obtain at least limiting values for the stability constant $K_S$ of the semi-reduced state and hence $\Delta E= E_1-E_2$ (which are related by $\log K_S = (E_1-E_2)*F/RT$). Two distinct approaches allow the deduction of $K_S$ and ΔE from the titration curve of the semi-reduced $Mo^V$ state. The traditional method proceeds through the determination of the fractional population of this state which is related to ΔE *via* the dependence shown in Fig. 4B. This approach is complicated for the case of Mo-*bis*PGD enzymes by the fact that Mo-cofactor occupancy in these enzymes commonly doesn't reach 100% and must thus be determined by independent methods. A different way to access the values of $K_S$ and ΔE, discussed by Robertson *et al*. [23], exploits the width of the bell-shaped titration curve of the semi-reduced state. As shown in Fig. 4A, this width can be converted into ΔE for values of ΔE > -100 mV. Since the width of the bell curve asymptotically tends towards roughly 68 mV for very negative ΔEs, it becomes virtually independent of ΔE below about -100 mV. At higher values, however, measuring the width directly permits calculating ΔE and $K_S$ without having to resort to quantifications of total Mo and $Mo^V$. The latter method proved particularly powerful for the case of the Aio variants as detailed below.

### *3.3. Placing a limit on the $K_S$ value of the $Mo^V$ state in WT Aio*

Equilibrium redox titrations (at pH 6) monitored by X-band EPR spectroscopy have been performed on samples of Aio. A tiny EPR spectrum attributable to a $Mo^V$ state was

observed (Fig. 3, black spectrum) and found to titrate at $E_m$ = +240 ± 10 mV (Fig. 4C, open squares). The observed changes on ambient potential were redox-reversible and therefore represent a genuine redox transition rather than degradation-induced phenomena. The observed titration behavior corresponds to the $Mo^{V}/Mo^{IV}$ transition of the cofactor. Since no decrease in signal size was observed while titrating the sample to more positive potentials (Fig. 4C, open squares) the $Mo^{VI}/Mo^{V}$ redox transition to the fully oxidized state must occur at higher potentials than were attainable in our equilibrium titrations using potassium ferricyanide as oxidant. The n=1 redox $Mo^{V}/Mo^{IV}$ transition observed at 240 mV by EPR may appear inconsistent with the optically determined 2-electron transition at 240 mV (measured on the $Mo^{VI}$ state) raising doubts whether the EPR- and optically monitored redox transitions correspond to the same electrochemical species. We therefore quantified the $Mo^{V}$ signal in the WT by double integration of the $Mo^{V}$ EPR spectrum.

Comparing this double integral to that obtained on the $Mo^{V}$ state of respiratory nitrate reductase (Nar, Fig. 3, orange curve) and correcting for experimental conditions and Mo content in Aio (quantified at around 80% by ICP-MS), we find that the maximal $Mo^{V}$ signal attained during our EPR titrations of WT (Fig. 4C), corresponds to only 2 % of total Mo present in the sample. According to the dependence shown in Fig. 4B, the population of the $Mo^{V}$ state in the maximum of the bell-curve of Fig. 4C should be close to 100 % of total cofactor of its harboring enzyme. We therefore conclude that a small fraction (2 %) of our sample features a very strongly stabilized intermediate redox state of the Mo-*bis*PGD cofactor. Whether this fraction corresponds to a non-physiological state or an alternative configuration of the enzyme cannot be decided at present. Whatever the origin of this minor fraction, the overwhelming majority (98 %) of Moco strongly destabilizes the $Mo^{V}$ state. The 2% contribution of the negative cooperativity redox transition as seen in EPR is by far too small to be detectable in our optical titration experiments (Fig. 2B). Since no other signal

attributable to $Mo^V$ was detected, the stabilisation of $Mo^V$ in the majority of enzymes (98 %) in the redox transition with strong positive cooperativity must be much smaller than the observed 2 % of the minority population with negative cooperativity. Taking 1% as an upper limit yields ΔE values below -200 mV (Fig. 4B) and $K_S < 4\times10^{-4}$. The degree of redox cooperativity in Aio can therefore be quantitatively expressed by these ΔE and $K_S$ values.

*3.4. Molecular determinants tuning redox cooperativity in Mo-bisPGD enzymes*

Redox cooperativity in quinones, the arguably most thoroughly studied class of 2-electron redox compounds [22], is generally considered to be mediated by the charge-compensating effect of protonation/deprotonation reactions [24] and/or hydrogen-bonding interactions [25] (see also our short introduction to the electrochemistry of 2-electron compounds in the Supplemental Material). It therefore is tempting to apply this paradigm also to Mo-*bis*PGD enzymes when searching for the parameters which steer the cofactor towards one redox regime or the other. We consequently looked for redox-coupled protonation/deprotonation events and/or redox-induced pK-changes as potentially cooperativity-tuning parameters. Fig. 5A shows a structure overlay of the ligand environment of the Mo-atom in Aio from *R.* sp. NT-26 to that of the Nar from *E. coli* for which stabilized $Mo^V$ states (at pH 8) have been reported [26-29]. Two fundamentally distinct locations in the environment of the Mo-ion feature intriguing structural differences possibly related to charge-compensating effects.

(1) The direct ligand sphere of the Mo atom. While in all representatives of the superfamily, four coordination sites of the Mo-ion are occupied by sulfur atoms provided in pairs by each of the two pyranopterins, the $5^{th}$ ligand to the Mo-atom is variable. It is an aspartate (Asp222) in Nar but can be serine or cysteine in other Mo-*bis*PGD enzymes whereas

the 6$^{th}$ coordination site appears to be reserved for the catalytic reaction, *i.e*. is occupied by an oxo-, hydroxo- or sulfur- group (for a recent review, see [30]). In the X-ray structures of Aio, however, the 5$^{th}$ coordination position on the Mo-ion is fully vacant (Fig. 5A). However, these structures have been obtained in the reduced state of the enzyme, which doesn't rule out differing conformations while the Mo center is oxidized. EXAFS and Raman studies indeed suggested the presence of a distended oxo or a hydroxo group as the 5$^{th}$ ligand in the oxidized state [31], in addition to the canonical oxo-ligand present in several other members of the superfamily. The stoichiometry of 2 protons per 2 electrons in Aio's redox transition prompted Hoke *et al.* [12] to favor the hypothesis that the additional oxygen ligand is indeed an oxo group and that reduction of the enzyme would entail double protonation of this oxo group, followed by dissociation of the produced water molecule. Such a reaction mechanism provides the essential ingredients for $H^+$-linked destabilization of the intermediate redox state as in the case of quinones.

To test this hypothesis we have generated variants of Aio potentially providing a 5$^{th}$ ligand to the Mo-atom. Sequence alignments of Aio and Nar suggest Ala203 of the *R*. sp. NT-26 Aio as the residue corresponding to the ligating Asp222 of Nar [32]. We have therefore replaced A203 by Ser, Cys and Asp to mimic ligand permutations so far observed in the superfamily. The A203S and A203C variants showed enzymatic and electrochemical properties similar to those of the WT enzyme (see Table 1) whereas the A203D variant had no detectable activity, was highly unstable and showed significantly modified UV/Vis-spectroscopic properties of the Mo-cofactor. The signal amplitude of the spectral contribution at 695 nm (Fig. S4) together with metal analysis results (5% Mo content quantified by ICP-MS) demonstrated that the Mo content of this variant was very low. We nevertheless were able to evaluate the redox properties of its residual Mo-center at pH 7 and determined an $E_m$

of + 140 mV (Table 1) and a positive cooperative 2-electron transition. No EPR signal attributable to $Mo^{V}$ was detected in any of the A203 variants (Fig. 3).

The data obtained for these variants thus do not straightforwardly support a link between absence of a protein ligand to the Mo-atom and Aio's unique redox properties. However, the similarity of the Cys and Ser variants to the WT enzyme (we verified all the variants by ESI/MS) raises doubts as to whether the Ser and Cys mutations have actually introduced a $5^{th}$ ligand to the Mo-atom. The structural overlay of corresponding sequence stretches in Aio and Nar shown in Fig. 5A (grey for Nar and blue for Aio) highlights a substantially different fold in Aio of the whole stretch of amino acids between sequence positions 199 (end of β-sheet) and 209 (beginning of α-helix). This modified conformation moves the amino acid corresponding to the ligand in Nar away from the Mo-atom. It therefore isn't obvious that the entire sequence stretch actually did restructure upon introduction of the potential Mo-ligand.

Concerning the A203D variant, two scenarios are conceivable. (a) As for the two other variants, the Asp residue remained too far from the Mo-center to become a ligand. The introduced negative charge positioned about 12 Å from the Mo-center induced an $E_m$ downshift due to electrostatic interaction. (b) The Asp residue became the $5^{th}$ Mo-ligand but the far-reaching reorganization of the flanking chain resulted in instability of cofactor binding. The introduction of a $5^{th}$ ligand would then have severely affected spectral properties and $E_m$, however without detectably shifting the redox transition towards the negative cooperativity regime.

Irrespective of whether a $5^{th}$ ligand has been introduced or not, it is worth noting that the scenario of a present/absent oxo-group at the $5^{th}$ ligating position as cooperativity-tuning parameter fails to provide a unifying mechanism for the redox behavior of the entire superfamily. As mentioned, Aio represents an extreme but not the only case of redox positive

cooperativity in this superfamily. Dor also does so but the 5$^{th}$ coordination site of its Mo-atom isn't vacant but occupied by an O atom from a Ser residue.

(2) The H-bonding network surrounding the pyranopterins: The four pyranopterin-sulfurs coordinating the Mo-atom (Fig. 5) are part of an extended conjugated system and electron density in the Mo-orbitals therefore may be influenced by even remote parts of the pterin moieties. Indeed, a role of the pyranopterins as "non-innocent" ligands has been increasingly discussed over recent years [33, 34]. In particular, the pyranopterins are embedded in an extensive H-bonding network provided by the ambient protein and are thus likely candidates for providing cooperativity-tuning charge compensation effects. We have therefore looked for inter-enzyme differences in the vicinity of the two pyranopterins. While the respective "outer" (*i.e.* pointing away from the Mo-center) protons on both pterins are H-bonded by backbone-amides in all structures of representatives from the superfamily, intriguing differences can be found with respect to the "inner" hydrogens (Fig. 5B). In the well-studied model system Nar, two prominent His residues have been proposed to engage in multiple H-bond interactions [33]. The so-called "bridging" His1092 provides a H-bond interconnection between the proximal (P) and the distal (D) pyranopterins while a "stabilizing" His1098 is considered to be crucial for fixing the P pyranopterin in its particular conformation [33]. The His1098 residue is indeed conserved in many members of the superfamily while His1092 is frequently replaced by an Arg (e.g. Arg720 in Aio, Fig. 5B) residue showing similar H-bond interactions. In the structural comparison of Aio and Nar shown in Fig. 5 as well as in comprehensive multiple sequence alignments of representatives of the superfamily [35], however, Aio stands out (together with an as yet uncharacterized enzyme from *Desulfovibrio gigas* and the acetylene hydratase from *Pelobacter acetylenicus* [36] by the presence of a glutamine residue (Gln726) in the position of the canonical stabilizing His (Fig. 5B). According to both available structures of Aio, the oxygen atom on

the Gln726 side-chain is a strong H-bond acceptor to the proton on the $N_5$ nitrogen of the P pyranopterin (Fig. 5A). The almost singular presence of this particular amino acid in a strategic position prompted us to assess its role in Aio's redox chemistry through site-directed mutagenesis. We therefore substituted Gln726 with a glycine residue which is unable to engage in hydrogen bond interactions from its side-chain.

This variant was found to feature prominent EPR lines in the spectral region characteristic for $Mo^V$ centers as shown in Fig. 3 (red spectrum) in addition to much smaller signals resembling those of the paramagnetic species already observed in the wild type (detected at high ambient potentials where the strong EPR signal is absent; see below and Table S2). The dominant spectrum is distinguishable from both that of the WT enzyme and that of Nar. Its spectral features do not arise from the [3Fe-4S]cluster which shows no measureable signal at 50K [17]. The Rieske [2Fe-2S] cluster, which indeed is still visible at 50K, is observed at lower redox potentials without contributions from the other centers and was subtracted out of the red spectrum shown in Fig. 3. None of the two iron-sulfur centers present in the enzyme thus contribute to this spectrum. Its saturation behavior was found to correspond to that of typical Mo-*bis*PGD centers (data not shown). As detailed below, the bell-shaped titration curve of this paramagnetic center resembles that of $Mo^V$ states in other members of the superfamily and the $E_1$ and $E_2$ values of the two redox transitions as obtained by EPR are fully consistent with the 2-electron potential measured by our optical approach. To obtain signal-to-noise ratios allowing for the identification of finer spectral structures, the spectrum shown in this figure was extensively accumulated (396 times). The spectral features indicated by asterisks in Fig. 3 most likely correspond to hyperfine lines arising from the minor $^{95}$Mo- and $^{97}$Mo-isotopes with nuclear spin I= 5/2. A literature survey suggests that the spectrum of our variant (see Table S2 for *g* values) most closely resembles that reported for $Mo^V$ in the enzyme Fdh from *Methanobacterium formicicum* [6]. The ensemble of these

observations therefore demonstrates that the observed spectrum indeed corresponds to the $Mo^V$ state in the variant enzyme.

The quality of the data points during the titration of the $Mo^V$ signal in the Q726G variant (Fig. 4C) allows a reliable determination of the full width at half maximum ($W_{HH}$) of this curve yielding a value of 93 mV (Fig. 4C) which translates into a ΔE of +36 mV and also to 45% stabilization of the $Mo^V$ state, according to the dependences illustrated in Fig. 4AB. This indicates that the variant enzyme stabilizes the $Mo^V$ state observable by EPR at cryogenic temperatures with $K_S = 4$ ($\log K_S = 0.6$) to the exception of the strongly stabilized fraction also observed in the WT. The Q726G mutation thus substantially stabilizes $Mo^V$ as compared to the WT.

According to the theoretical titration curves (Fig. S2B), a Mo redox behavior with ΔE +36 mV as observed by low temperature EPR should also give rise to deviations from n=2 behavior detectable in room temperature optical titrations of the $Mo^{VI}$ state. Fig. 2C shows the result of such an optical titration on the Q726G variant (see inset for comparison of the spectrum recorded on Q726G with the one from the WT). While the data points in the variant (Fig. 2C) clearly show a shallower dependence of the signal amplitude on ambient redox potential than in the WT (Fig. 2B), they do not yet approach n=1 behavior as predicted from the simulations (Fig. S2B). Fitting the data to the equation given in Supplementary Material as formulated by Clark [22], yields a ΔE of -44 mV, *i.e*. much higher than the limiting value of -200 mV found in the WT but indisputably lower than the EPR value of +36 mV. Previous results reported for Dor suggest a straightforward rationalization for this discrepancy. Bastian *et al*. [7] have analyzed the redox behavior of the $Mo^V$ state both at 298 K and at 168 K and have found appreciable but dissimilar temperature dependences for the two individual 1-electron transitions. While $E_1$ was observed to be constant within experimental precision, $E_2$ increased by about 60 mV when analyzed at cryogenic temperatures. In Aio, both transitions

appear to be temperature-dependent with $E_1$ increasing by about 40 mV and $E_2$ decreasing by the same amount when going to low temperatures. In the framework of the scenario that the Mo-cofactor's redox properties are controlled by the H-bonding network surrounding the pyranopterins as suggested by our mutagenesis results and as discussed in more detail below, differences in the effect of temperature on the individual 1-electron transitions find an explanation in differential modifications of the pK values on involved protonation sites. The pK values of numerous protonable/deprotonable groups are in fact temperature-dependent[37].

## 4. Discussion

### *4.1. On the complementarities of the optical and the EPR approaches*

The data concerning the Q726G variant detailed above together with previous results on Dor demonstrate that both individual redox transitions can feature temperature-dependent redox potentials. This potentially influences the apparent overall 2-electron midpoint potential, the stability constant $K_S$ of the semi-reduced state or both these parameters. Obviously, catalytic turnover is always determined above 0 $^{o}$C and electrochemical parameters determined at cryogenic temperatures may therefore be misleading in certain cases when correlated with enzyme activities. This fact adds to the potential of the optically monitored equilibrium redox titration approach. Not only will this approach always produce 2-electron $E_m$-values applicable to the conditions of enzyme assays but it allows, as shown above, to also determine the $E_1$ and $E_2$-values of the individual 1-electron transitions down to potential inversions $\Delta E$ of about -50 mV. Obtaining equivalent information from room

temperature titrations of the EPR detectable $Mo^V$ state requires substantially higher enzyme concentrations which are not always attainable.

*4.2. The H-bond environment of the pyranopterins controls the Mo-cofactor's redox behavior*

The comparison of the results obtained on the WT and the Q726G enzymes demonstrates that the electrochemical parameters of both redox transitions of the Mo-cofactor are strongly influenced by the H-bonding environment of the pyranopterins. Elimination of the H-bond relay provided by Gln726 in Aio affects both $E_1$ and $E_2$ and results in an increased stabilization of the $Mo^V$ state, by four orders of magnitude. Remarkably, the results published by Wu *et al*. during the course of our work [38] show that similar phenomena occur in Nar. The substitution of His1098, structurally equivalent to the Gln726 residue in Aio, by an Ala also substantially increases the stability of the $Mo^V$ state ($K_S$ from 28 for the WT to 1822 for the H1098A variant). Variants of other H-bonding His only led to marginal stabilization or even destabilized the $Mo^V$ state [38]. The fully congruent results obtained on Nar and on Aio emphasize the preeminent importance of the H-bond interactions provided by the amino acid residues at this specific structural/sequence position in the protein and we predict that mutagenesis work on other members of the superfamily will reveal a corresponding influence of the H-bond environment of the pyranopterins in the control of the Mo-cofactor's redox behavior.

*4.3. The variability of redox cooperativity in the Mo-bisPGD cofactors resembles that of quinones*

519 The relationship between $\Delta E = E_1\text{-}E_2$ and $K_S$ in 2-electron redox compounds is most
520 conveniently visualized by the type of plot shown in Fig. 6, *i.e*. the graphical representation of
521 the relationship $\log K_S = (E_1\text{-}E_2)*F/RT$, introduced by Mitchell as "the redox seesaw" [39]. In
522 many Mo-*bis*PGD enzymes such as *Rhodobacter sphaeroides* f. sp. *denitrificans*
523 Dimethylsulfoxide reductase Dms, *Rhodovulum sulfidophilum* Dimethylsulfide
524 dehydrogenase Ddh, *E. coli* Nar and *M. formicicum* Formate dehydrogenase Fdh [6, 8, 10,
525 27], positive ΔE values in the range of +100 mV (violet arrows in Fig. 6) and even as high as
526 775 mV for periplasmic nitrate reductase Nap [9] (out of range in Fig. 6) have been
527 determined. The redox properties of these enzymes thus clearly fall within the regime of
528 negative cooperativity. However, not all of them do, for *E. coli* Nar [11] a ΔE as low as +40
529 mV has been reported at pH 7.6. As already mentioned, in Dor from *Rhodobacter*
530 *sphaeroides*, the $E_1$ and $E_2$ values are inverted by almost -60 mV at pH 7 (corresponding to
531 $\log K_S = -1$) [7]. In these cases the individual 1-electron redox transitions therefore show
532 weakly, to substantially positive, redox cooperativity. The case of Aio extends the range of
533 accessible 2-electron electrochemical behavior of the Mo-*bis*PGD cofactor far into the regime
534 of positive cooperativity with $\log K_S$ below -3.

535 For comparison, the redox patterns of selected quinones as observed in biological
536 systems (brown arrows) [40-43] are indicated in Fig. 6. This pattern ranges from the strongly
537 negative cooperative behavior of the menaquinone in Nar [40] ($\log K_S \sim +2$) to that of the so-
538 called $Q_o$-site quinone of $bc_1$ complexes [44, 45] ($\log K_S = -14$, out of range in Fig. 6). In the
539 case of quinones, charge-compensating effects of protonation/deprotonation reactions [24]
540 and/or hydrogen-bonding interactions [25] have been put forward to explain modulation of
541 redox cooperativity. The Mo-*bis*PGD cofactors' redox properties thus resemble those of
542 quinones.

543

### *4.4. Repercussions on the role of Mo in early life*

Species distribution analyses and phylogenetic reconstructions indicate a very deep ancestry of the Mo-*bis*PGD superfamily dating back to early life [35]. We have in the past speculated that the transition metal Mo may, during life's inorganic infancy, have performed the positive cooperative (n=2) redox reactions crucial to bioenergetics [46, 47] which subsequently have been assumed by small organic molecules such as quinones and flavins [35, 48-50]. However, the finding that the redox cooperativity in Mo-enzymes is induced by the environment of the pyranopterin ligands suggests that respective protonatable groups were likely also present in the Mo-bearing minerals involved in the emergence of the earliest metabolic reactions. This observation favors as promising candidates the mixed and variable valence double layer oxyhydroxides such as hydrotalcite or green rust, the interlayers of which are readily protonated and deprotonated [51]. In this state they can contain various counter-ions including molybdates and thiomolybdates [52, 53]. Soluble mixed $Mo^{IV}$ oxide and sulfide complexes could have been supplied to the interlayers from the alkaline hydrothermal fluid and alternately oxidized and reduced therein [54]. Whether there are circumstances in which oxidation and reduction of these complexes could have involved 2-electron redox behavior with positive cooperativity is not known but is ripe for experimentation.

## Author Contributions

J.M.S. carried out the molecular biology, S.D. and B.S.C. carried out the biochemical and optical spectroscopy experiments, S.D., B.S.C. and S.G. carried out the EPR experiments.

D.L. carried out the ESI/MS analyses, F.C. carried out the ICP/MS analyses. S.D., B.S.C., S.G. and W.N. analyzed the data. All authors wrote the paper.

## Acknowledgments

We thank Axel Magalon and Frédéric Biaso for helpful discussions and Pierre Ceccaldi for Nar preparation. Our work is funded by the CNRS, CEA, Aix-Marseille Université, ANR (Project MC2, 11-BSV5-005-01). MJR's research was carried out at the Jet Propulsion Laboratory, California Institute of Technology, under a contract with the National Aeronautics and Space Administration and with support by the NASA Astrobiology Institute (Icy Worlds). The authors are grateful to the EPR facilities available at the Aix-Marseille University EPR center, and to financial support from the French EPR network (RENARD, IR3443).

## Supplementary data

Supplementary data to this article can be found online at http:…

## Legends

**Figure 1.** Values and pH dependences of the Mo-cofactor's redox potentials. Blue squares and the blue continuous line (representing an $H^+/e^-$ ratio of 1) represent the results obtained in the present work on the *R.* sp. NT-26 Aio. The blue dotted line indicates the data reported by Bernhardt and Santini [13] on the *R.* sp. NT-26 Aio, simulated with an $H^+/e^-$ ratio of 0.5. Orange triangles mark the results obtained in the present work on the heterologously expressed *A. faecalis* enzyme. The red dotted line corresponds to the data reported by Hoke *et al*. [12] on the native *A. faecalis* Aio.

**Figure 2**. Optical titration of the Mo-cofactor in wild type Aio and the Q726G variant from *R.* NT-26. A: Optical spectra recorded on the wild type enzyme in the region 600-800 nm, recorded at pH6 during titrations. B: Dependence of signal amplitudes on ambient redox potential as evaluated at 695 nm and fitted with Nernstian sigmoids using $E_m$= +240 mV and n=2 (blue) or n=1 (red) behavior. The figure summarizes data obtained in two consecutive cycles of reductive and oxidative titrations. The experiment has been repeated twice independently on different enzyme preparations. C: Evaluation of signal amplitudes at 705 nm recorded during redox titrations of the Q726G variant. Dashed blue and red lines correspond to n=2 and n=1 behavior, respectively, as in B, while the continuous black line results from a fit of the data points to the theoretical dependence of the $Mo^{VI}$ state towards ambient redox potential. The inset shows the comparison of the optical spectrum recorded on the WT enzyme (blue line) to that recorded on the Q726G variant (black line).

**Figure 3.** EPR spectra recorded on wild type and variant Aio from *R.* sp. NT-26 as well as on *E. coli* Nar. Approximately 45 µM enzyme were used for redox titrations at pH 6 (for WT, A203C and Q726G enzymes) or pH 7 (for the A203D variant). Spectra were recorded on samples poised at +240 mV at pH 6 in the case of WT, A203C and Q726G and at +140 mV at pH 7 in the case of A203D. In the spectrum recorded on the Q726G enzyme, the spectral features indicated by asterisks most likely correspond to hyperfine lines arising from the minor $^{95}$Mo- and $^{97}$Mo-isotopes with nuclear spin I= 5/2. Spectra recorded on Aios are compared to the spectrum recorded on NarGH purified from *E. coli* and poised at +155 mV at pH 7.6. Numbers 1, 2 and 3 denote $g_{1,2,3}$ values associated with each of the signals. The chosen experimental conditions allow detecting the Mo

cofactor of Nar in the $Mo^V$ state. All spectra were recorded at a microwave frequency of 9.48 GHz, a microwave power of 1 mW, a temperature of 50K and a modulation amplitude of 0.4 mT.

**Figure 4.** Theoretical dependences of the full width at half maximum ($W_{HH}$) of the $Mo^V$-titration curve (A) and of the maximally observable $Mo^V$ signal (B) on the difference in individual 1-electron redox potentials ($\Delta E = E_1 - E_2$). C: Experimentally determined titration curves for the weak $Mo^V$ signal observed in the wild type enzyme (open squares) and the prominent $Mo^V$ spectrum of the Q726G variant (filled diamonds). For a detailed presentation of the equations describing 2-electron redox transitions, see the tutorial included in the Supplemental Material or visit our dedicated website at http://bip.cnrs-mrs.fr/bip09/2electron.html.

**Figure 5.** Structure comparison of Aio and Nar enzymes. A: Comparative juxtaposition of the 3D-structures of Aio from *R.* sp. NT-26 (in blue) and of Nar from *E. coli*. (in grey). Crucial amino acid residues, the two pyranopterins and protonatable positions on the pterins are highlighted. B: Comparison of the proximal and distal pyranopterins and crucial interacting amino acid residues in Nar (grey) and Aio (blue) as seen from "below" the Mo-*bis*PGD moiety.

**Figure 6**. "Redox-seesaw" representation of the dependence of $\Delta E = (E_1 - E_2)$ on the stability constant $K_S$ of the half-reduced state. Experimentally determined values for semiquinones (in brown) or $Mo^V$ (in violet) intermediates are represented. The red arrow stands for the values determined in this work for the Q726G variant of Aio.

**Table 1.** Properties of wild type and variant Aio enzymes from *R.* NT26 and *A. faecalis*. Except for the Q726G variant, the redox potential value represents the $E_m$ value of the 2-electron redox transitions. In the case of Q726G, $E_1$ and $E_2$ can be distinguished and are indicated.

## References

[1] R. Hille, The Mononuclear Molybdenum Enzymes, Chemical reviews, 96 (1996) 2757-2816.
[2] R.A. Rothery, G.J. Workun, J.H. Weiner, The prokaryotic complex iron-sulfur molybdoenzyme family, Biochimica et biophysica acta, 1778 (2008) 1897-1929.
[3] R. van Lis, W. Nitschke, S. Duval, B. Schoepp-Cothenet, Arsenics as bioenergetic substrates, Biochimica et biophysica acta, 1827 (2013) 176-188.

[4] P.J. Ellis, T. Conrads, R. Hille, P. Kuhn, Crystal structure of the 100 kDa arsenite oxidase from Alcaligenes faecalis in two crystal forms at 1.64 A and 2.03 A, Structure, 9 (2001) 125-132.
[5] T.P. Warelow, M. Oke, B. Schoepp-Cothenet, J.U. Dahl, N. Bruselat, G.N. Sivalingam, S. Leimkuhler, K. Thalassinos, U. Kappler, J.H. Naismith, J.M. Santini, The respiratory arsenite oxidase: structure and the role of residues surrounding the rieske cluster, PloS one, 8 (2013) e72535.
[6] M.J. Barber, L.M. Siegel, N.L. Schauer, H.D. May, J.G. Ferry, Formate dehydrogenase from Methanobacterium formicicum. Electron paramagnetic resonance spectroscopy of the molybdenum and iron-sulfur centers, The Journal of biological chemistry, 258 (1983) 10839-10845.
[7] N.R. Bastian, C.J. Kay, M.J. Barber, K.V. Rajagopalan, Spectroscopic studies of the molybdenum-containing dimethyl sulfoxide reductase from Rhodobacter sphaeroides f. sp. denitrificans, The Journal of biological chemistry, 266 (1991) 45-51.
[8] N.L. Creevey, A.G. McEwan, G.R. Hanson, P.V. Bernhardt, Thermodynamic characterization of the redox centers within dimethylsulfide dehydrogenase, Biochemistry, 47 (2008) 3770-3776.
[9] V. Fourmond, B. Burlat, S. Dementin, P. Arnoux, M. Sabaty, S. Boiry, B. Guigliarelli, P. Bertrand, D. Pignol, C. Leger, Major Mo(V) EPR signature of Rhodobacter sphaeroides periplasmic nitrate reductase arising from a dead-end species that activates upon reduction. Relation to other molybdoenzymes from the DMSO reductase family, The journal of physical chemistry. B, 112 (2008) 15478-15486.
[10] R.A. Rothery, C.A. Trieber, J.H. Weiner, Interactions between the molybdenum cofactor and iron-sulfur clusters of Escherichia coli dimethylsulfoxide reductase, The Journal of biological chemistry, 274 (1999) 13002-13009.
[11] S.P. Vincent, Oxidation--reduction potentials of molybdenum and iron--sulphur centres in nitrate reductase from Escherichia coli, The Biochemical journal, 177 (1979) 757-759.
[12] K.R. Hoke, N. Cobb, F.A. Armstrong, R. Hille, Electrochemical studies of arsenite oxidase: an unusual example of a highly cooperative two-electron molybdenum center, Biochemistry, 43 (2004) 1667-1674.
[13] P.V. Bernhardt, J.M. Santini, Protein film voltammetry of arsenite oxidase from the chemolithoautotrophic arsenite-oxidizing bacterium NT-26, Biochemistry, 45 (2006) 2804-2809.
[14] P. Lanciano, A. Vergnes, S. Grimaldi, B. Guigliarelli, A. Magalon, Biogenesis of a respiratory complex is orchestrated by a single accessory protein, The Journal of biological chemistry, 282 (2007) 17468-17474.
[15] P.L. Dutton, Oxidation-reduction potential dependence of the interaction of cytochromes, bacteriochlorophyll and carotenoids at 77 degrees K in chromatophores of Chromatium D and Rhodopseudomonas gelatinosa, Biochimica et biophysica acta, 226 (1971) 63-80.
[16] S. Duval, J.M. Santini, W. Nitschke, R. Hille, B. Schoepp-Cothenet, The small subunit AroB of arsenite oxidase: lessons on the [2Fe-2S] Rieske protein superfamily, The Journal of biological chemistry, 285 (2010) 20442-20451.
[17] G.L. Anderson, J. Williams, R. Hille, The purification and characterization of arsenite oxidase from Alcaligenes faecalis, a molybdenum-containing hydroxylase, The Journal of biological chemistry, 267 (1992) 23674-23682.
[18] R.C. Bray, B. Adams, A.T. Smith, R.L. Richards, D.J. Lowe, S. Bailey, Reactions of dimethylsulfoxide reductase in the presence of dimethyl sulfide and the structure of the dimethyl sulfide-modified enzyme, Biochemistry, 40 (2001) 9810-9820.
[19] F.A. Leitch, K.R. Brown, G.W. Pettigrew, Complexity in the redox titration of the dihaem cytochrome c4, Biochimica et biophysica acta, 808 (1985) 213-218.
[20] D.L. Turner, C.A. Salgueiro, T. Catarino, J. Legall, A.V. Xavier, NMR studies of cooperativity in the tetrahaem cytochrome c3 from Desulfovibrio vulgaris, European journal of biochemistry / FEBS, 241 (1996) 723-731.
[21] L. Michaelis, Theory of the reversible two-step oxidation, The Journal of biological chemistry, 96 (1932) 703-715.

690 [22] W.M. Clark, Modification of primary equations to account for the formation of intermediate free
691 radicals, "semiquinones", in: Oxidation-reduction potentials of organic systems, The Williams and
692 Wilkins Company, Baltimore, 1960, pp. 184-203.
693 [23] D.E. Robertson, R.C. Prince, J.R. Bowyer, K. Matsuura, P.L. Dutton, T. Ohnishi, Thermodynamic
694 properties of the semiquinone and its binding site in the ubiquinol-cytochrome c (c2) oxidoreductase
695 of respiratory and photosynthetic systems, The Journal of biological chemistry, 259 (1984) 1758-
696 1763.
697 [24] M.R. Gunner, J. Madeo, Z. Zhu, Modification of quinone electrochemistry by the proteins in the
698 biological electron transfer chains: examples from photosynthetic reaction centers, Journal of
699 bioenergetics and biomembranes, 40 (2008) 509-519.
700 [25] M. Quan, D. Sanchez, M.F. Wasylkiw, D.K. Smith, Voltammetry of quinones in unbuffered
701 aqueous solution: reassessing the roles of proton transfer and hydrogen bonding in the aqueous
702 electrochemistry of quinones, Journal of the American Chemical Society, 129 (2007) 12847-12856.
703 [26] S.J. Field, N.P. Thornton, L.J. Anderson, A.J. Gates, A. Reilly, B.J. Jepson, D.J. Richardson, S.J.
704 George, M.R. Cheesman, J.N. Butt, Reductive activation of nitrate reductases, Dalton transactions,
705 (2005) 3580-3586.
706 [27] B. Guigliarelli, M. Asso, C. More, V. Augier, F. Blasco, J. Pommier, G. Giordano, P. Bertrand, EPR
707 and redox characterization of iron-sulfur centers in nitrate reductases A and Z from Escherichia coli.
708 Evidence for a high-potential and a low-potential class and their relevance in the electron-transfer
709 mechanism, European journal of biochemistry / FEBS, 207 (1992) 61-68.
710 [28] A. Magalon, M. Asso, B. Guigliarelli, R.A. Rothery, P. Bertrand, G. Giordano, F. Blasco,
711 Molybdenum cofactor properties and [Fe-S] cluster coordination in Escherichia coli nitrate reductase
712 A: investigation by site-directed mutagenesis of the conserved his-50 residue in the NarG subunit,
713 Biochemistry, 37 (1998) 7363-7370.
714 [29] R.A. Rothery, M.G. Bertero, R. Cammack, M. Palak, F. Blasco, N.C. Strynadka, J.H. Weiner, The
715 catalytic subunit of Escherichia coli nitrate reductase A contains a novel [4Fe-4S] cluster with a high-
716 spin ground state, Biochemistry, 43 (2004) 5324-5333.
717 [30] S. Grimaldi, B. Schoepp-Cothenet, P. Ceccaldi, B. Guigliarelli, A. Magalon, The prokaryotic Mo/W-
718 bisPGD enzymes family: a catalytic workhorse in bioenergetic, Biochimica et biophysica acta, 1827
719 (2013) 1048-1085.
720 [31] T. Conrads, C. Hemann, G.N. George, I.J. Pickering, R.C. Prince, R. Hille, The active site of arsenite
721 oxidase from Alcaligenes faecalis, Journal of the American Chemical Society, 124 (2002) 11276-
722 11277.
723 [32] J.F. Stolz, P. Basu, J.M. Santini, R.S. Oremland, Arsenic and selenium in microbial metabolism,
724 Annual review of microbiology, 60 (2006) 107-130.
725 [33] R.A. Rothery, J.H. Weiner, Shifting the metallocentric molybdoenzyme paradigm: the importance
726 of pyranopterin coordination, Journal of biological inorganic chemistry : JBIC : a publication of the
727 Society of Biological Inorganic Chemistry, 20 (2014) 349-372.
728 [34] B.R. Williams, Y. Fu, G.P. Yap, S.J. Burgmayer, Structure and reversible pyran formation in
729 molybdenum pyranopterin dithiolene models of the molybdenum cofactor, Journal of the American
730 Chemical Society, 134 (2012) 19584-19587.
731 [35] B. Schoepp-Cothenet, R. van Lis, P. Philippot, A. Magalon, M.J. Russell, W. Nitschke, The
732 ineluctable requirement for the trans-iron elements molybdenum and/or tungsten in the origin of
733 life, Scientific reports, 2 (2012) 263.
734 [36] R.A. Rothery, B. Stein, M. Solomonson, M.L. Kirk, J.H. Weiner, Pyranopterin conformation
735 defines the function of molybdenum and tungsten enzymes, Proceedings of the National Academy of
736 Sciences of the United States of America, 109 (2012) 14773-14778.
737 [37] D.L. Williams-Smith, R.C. Bray, M.J. Barber, A.D. Tsopanakis, S.P. Vincent, Changes in apparent
738 pH on freezing aqueous buffer solutions and their relevance to biochemical electron-paramagnetic-
739 resonance spectroscopy, The Biochemical journal, 167 (1977) 593-600.
740 [38] S.Y. Wu, R.A. Rothery, J.H. Weiner, Pyranopterin Coordination Controls Molybdenum
741 Electrochemistry in Escherichia coli Nitrate Reductase, The Journal of biological chemistry, (2015).

[39] P. Mitchell, Vectorial chemistry and the molecular mechanics of chemiosmotic coupling: power transmission by proticity, Biochemical Society transactions, 4 (1976) 399-430.
[40] S. Grimaldi, P. Lanciano, P. Bertrand, F. Blasco, B. Guigliarelli, Evidence for an EPR-detectable semiquinone intermediate stabilized in the membrane-bound subunit NarI of nitrate reductase A (NarGHI) from Escherichia coli, Biochemistry, 44 (2005) 1300-1308.
[41] G. Hauska, E. Hurt, N. Gabellini, W. Lockau, Comparative aspects of quinol-cytochrome c/plastocyanin oxidoreductases, Biochimica et biophysica acta, 726 (1983) 97-133.
[42] A.W. Rutherford, M.C. Evans, Direct measurement of the redox potential of the primary and secondary quinone electron acceptors in Rhodopseudomonas sphaeroides (wild-type) by EPR spectrometry, FEBS letters, 110 (1980) 257-261.
[43] M. Sato-Watanabe, S. Itoh, T. Mogi, K. Matsuura, H. Miyoshi, Y. Anraku, Stabilization of a semiquinone radical at the high-affinity quinone-binding site (QH) of the Escherichia coli bo-type ubiquinol oxidase, FEBS letters, 374 (1995) 265-269.
[44] A.R. Crofts, S. Hong, C. Wilson, R. Burton, D. Victoria, C. Harrison, K. Schulten, The mechanism of ubihydroquinone oxidation at the Qo-site of the cytochrome bc1 complex, Biochimica et biophysica acta, 1827 (2013) 1362-1377.
[45] H. Zhang, A. Osyczka, P.L. Dutton, C.C. Moser, Exposing the complex III Qo semiquinone radical, Biochimica et biophysica acta, 1767 (2007) 883-887.
[46] B. Schoepp-Cothenet, R. van Lis, A. Atteia, F. Baymann, L. Capowiez, A.L. Ducluzeau, S. Duval, F. ten Brink, M.J. Russell, W. Nitschke, On the universal core of bioenergetics, Biochimica et biophysica acta, 1827 (2013) 79-93.
[47] E. Branscomb, M.J. Russell, Turnstiles and bifurcators: the disequilibrium converting engines that put metabolism on the road, Biochimica et biophysica acta, 1827 (2013) 62-78.
[48] W. Nitschke, S.E. McGlynn, E.J. Milner-White, M.J. Russell, On the antiquity of metalloenzymes and their substrates in bioenergetics, Biochimica et biophysica acta, 1827 (2013) 871-881.
[49] W. Nitschke, M.J. Russell, Hydrothermal focusing of chemical and chemiosmotic energy, supported by delivery of catalytic Fe, Ni, Mo/W, Co, S and Se, forced life to emerge, J Mol Evol, 69 (2009) 481-496.
[50] W. Nitschke, M.J. Russell, Redox bifurcations: mechanisms and importance to life now, and at its origin: a widespread means of energy conversion in biology unfolds, BioEssays : news and reviews in molecular, cellular and developmental biology, 34 (2012) 106-109.
[51] J.M.R. Génin, R. C., C. Upadhyay, Structure and thermodynamics of ferrous, stoichiometric and ferric oxyhydroxycarbonate green rusts; redox flexibility and fougerite mineral, Solid State Sciences, 8 (2006) 1330-1343.
[52] C.E. Ciocan, E. Dumitriu, T. Cacciaguerra, F. Fajula, V. Hulea, New approach for synthesis of Mo-containing LDH based catalysts, Catalysis Today, 198 (2012) 239-245.
[53] A. Davantès, G. Lefèvre, In situ real time infrared spectroscopy of sorption of (poly) molybdate ions into layered double hydroxides, Journal of Physics and Chemistry A, 117 (2013) 12922-12929.
[54] G.R. Helz, B.E. Erickson, T.P. Vorlicek, Stabilities of thiomolybdate complexes of iron; implications for retention of essential trace elements (Fe, Cu, Mo) in sulfidic waters, Metallomics : integrated biometal science, 6 (2014) 1131-1140.

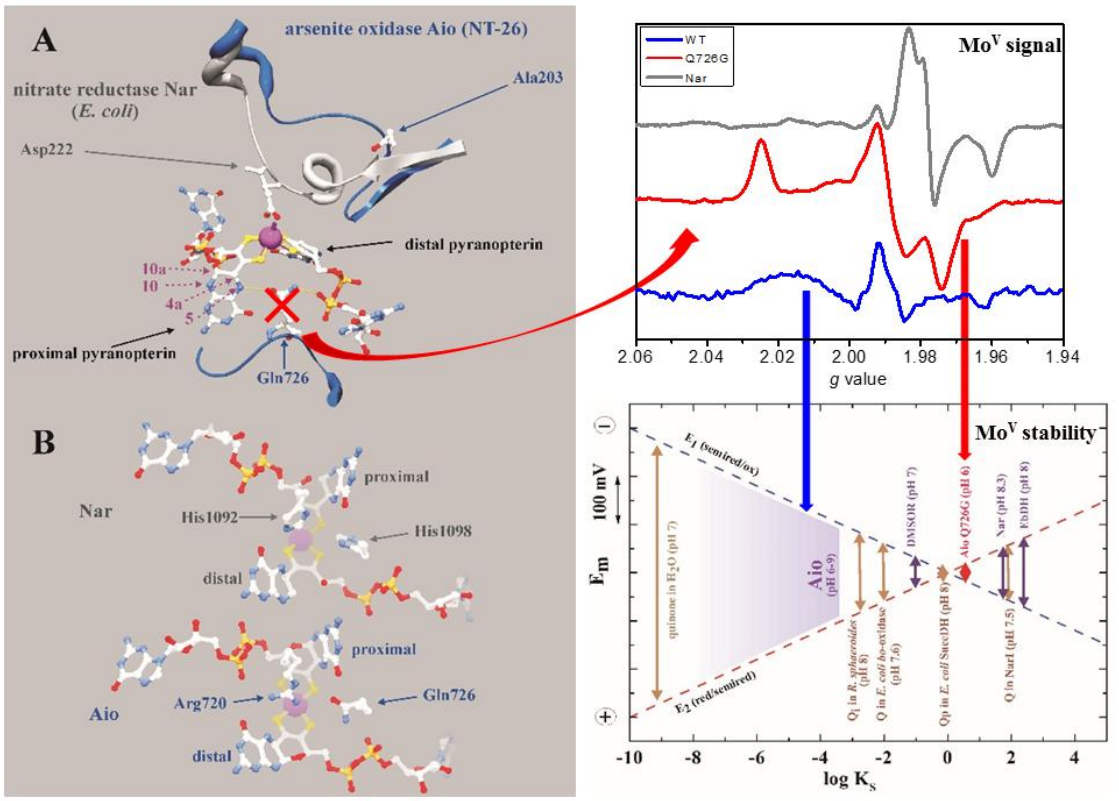


783

784 Graphical abstract

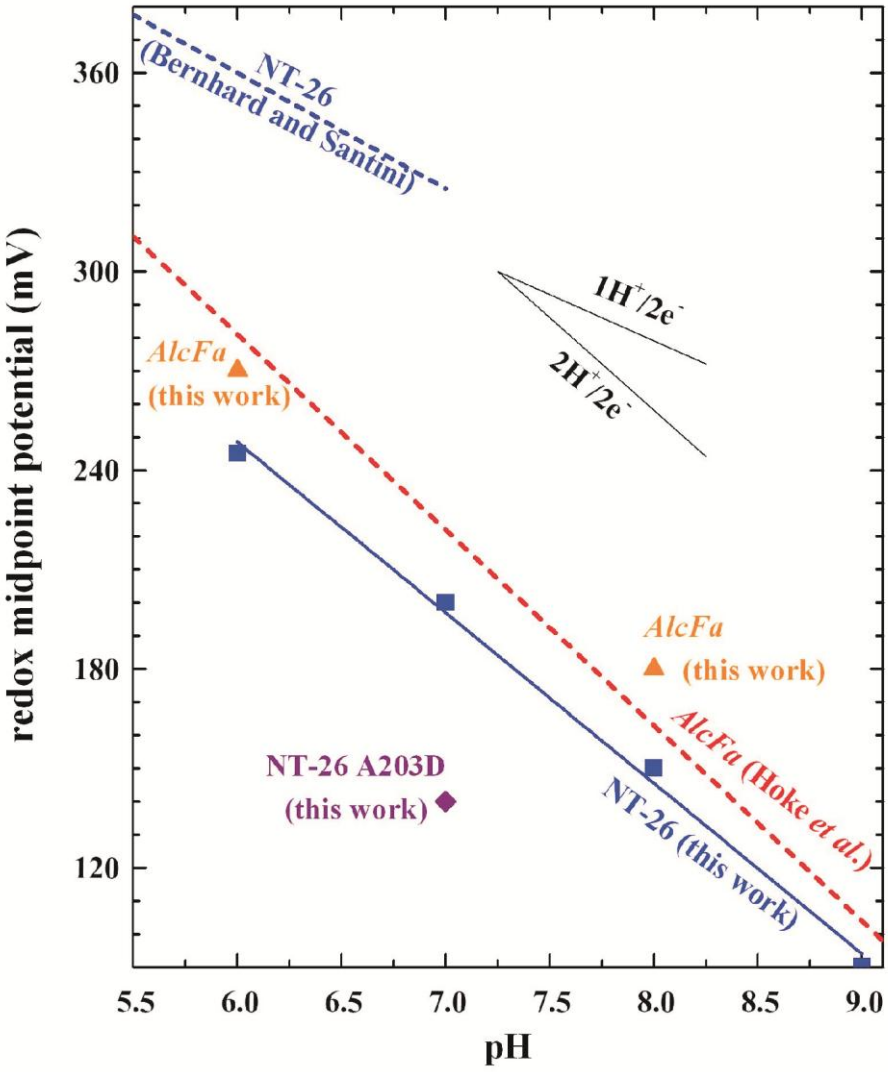


785

786 Fig. 1

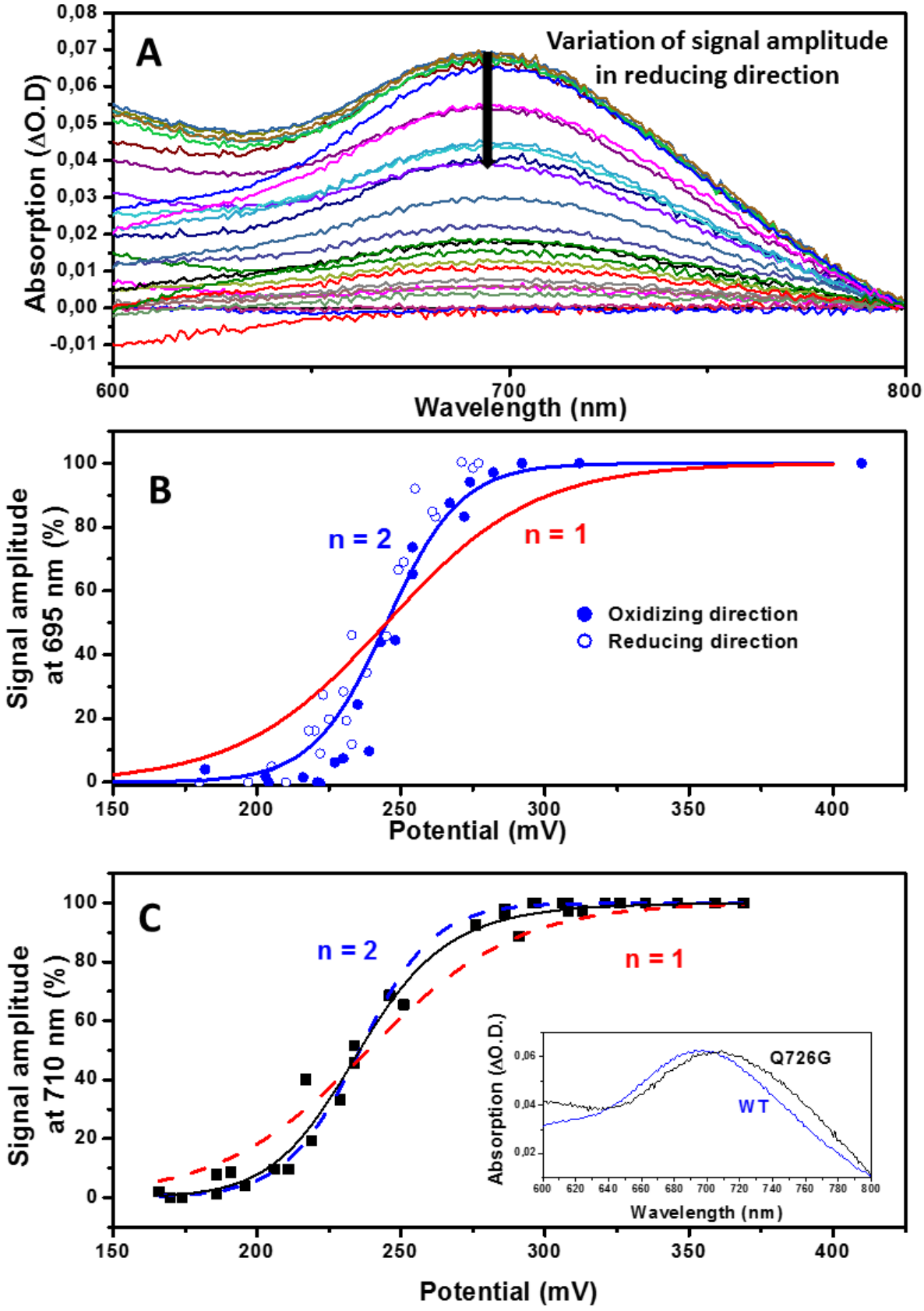


787

788 Fig. 2

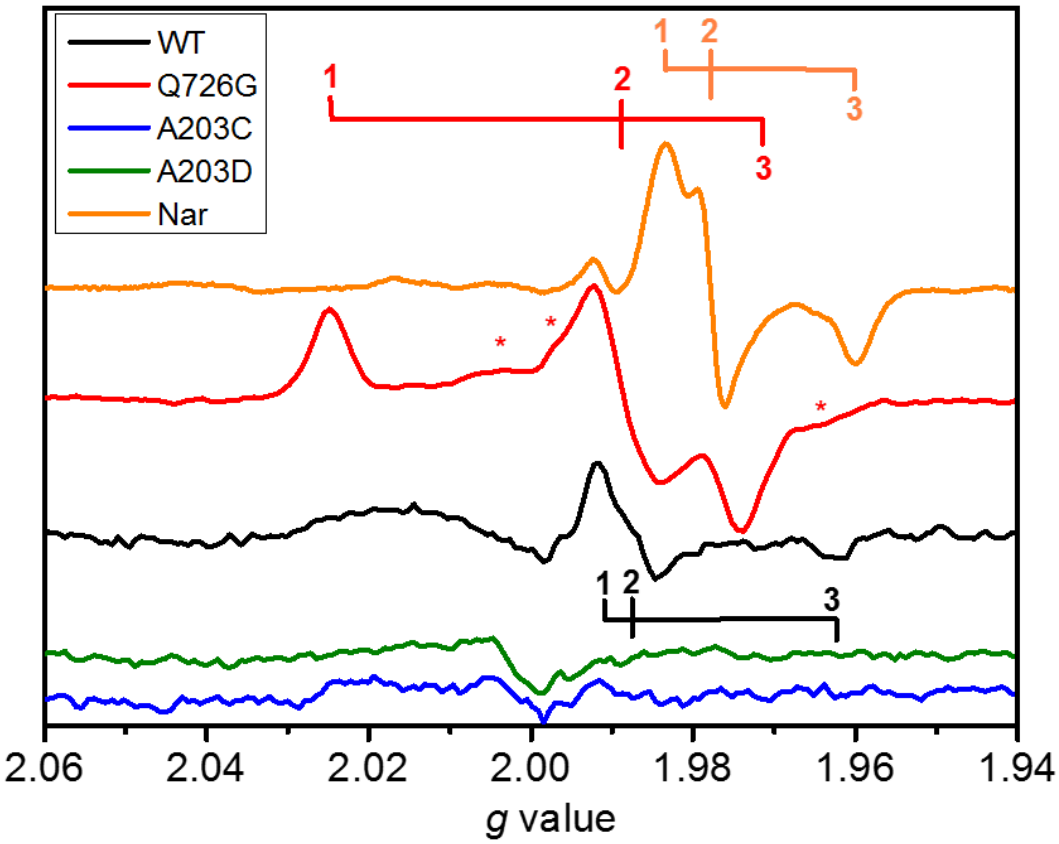


789

790 Fig. 3

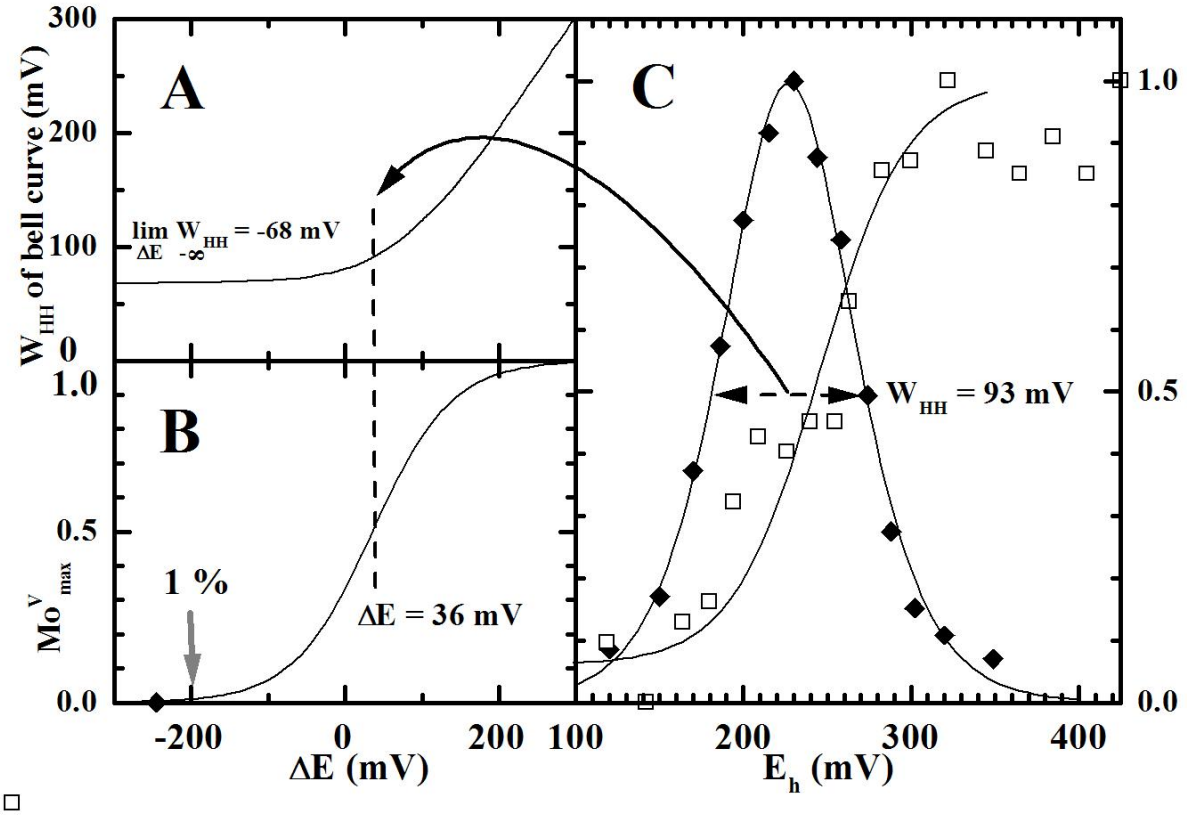


791 □

792 Fig. 4

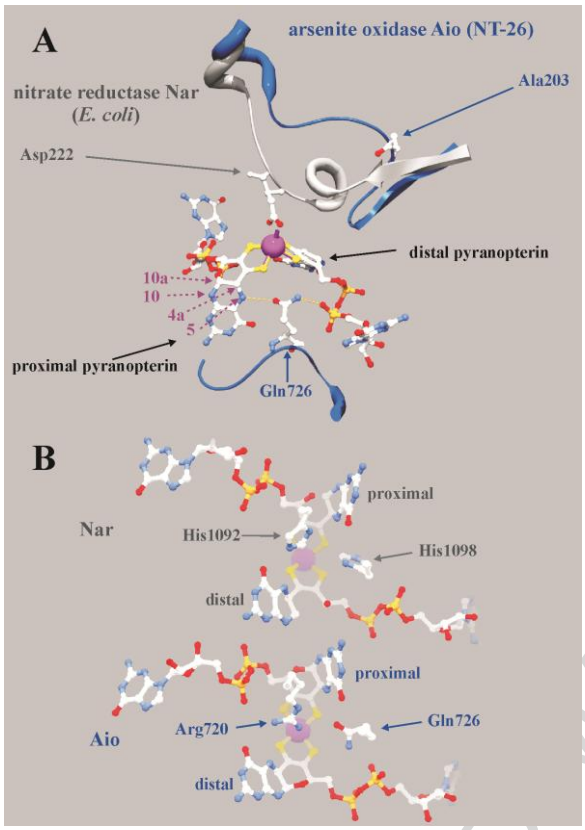


793

794 Fig. 5

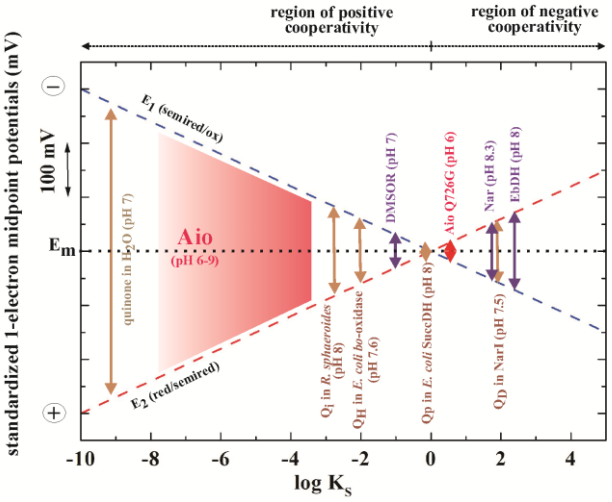


795

796 Fig. 6

797 Table 1

| Enzyme | Specific activity ($\mu$mol DCPIP.min$^{-1}$.mg$^{-1}$) | Midpoint potential (mV) Mo-center 50K | Midpoint potential (mV) Mo-center 286K | | | |
|---|---|---|---|---|---|---|
| | | pH6 | pH6 | pH7 | pH8 | pH9 |
| *R.* NT26 : | | | | | | |
| WT | 1.1 | nd | +240 | +200 | +150 | +90 |
| A203S | 0.88 | nd | +240 | -- | -- | -- |
| A203C | 1.1 | nd | +240 | -- | -- | -- |
| A203D | 0 | nd | -- | +140 | -- | -- |
| Q726G | 1.05 | $E_m$= +230<br>$E_1$=+248<br>$E_2$=+212 | $E_m$=+230<br>$E_1$=+208<br>$E_2$=+252 | -- | N.D | -- |
| *A. faecalis :* | | | | | | |
| WT | 2.5 | | +270 | -- | +180 | -- |

798

799

800 **Highlights**

801 - The Mo-*bis*PGD enzyme arsenite oxidase displays strong redox cooperativity

802 - Optical titrations appear as a powerful method for assessing Mo-redox properties

803 -The H-bond network surrounding the pyranopterins-ligands modulates cooperativity

804 - The Mo-*bis*PGD cofactor resembles quinones with respect to redox properties